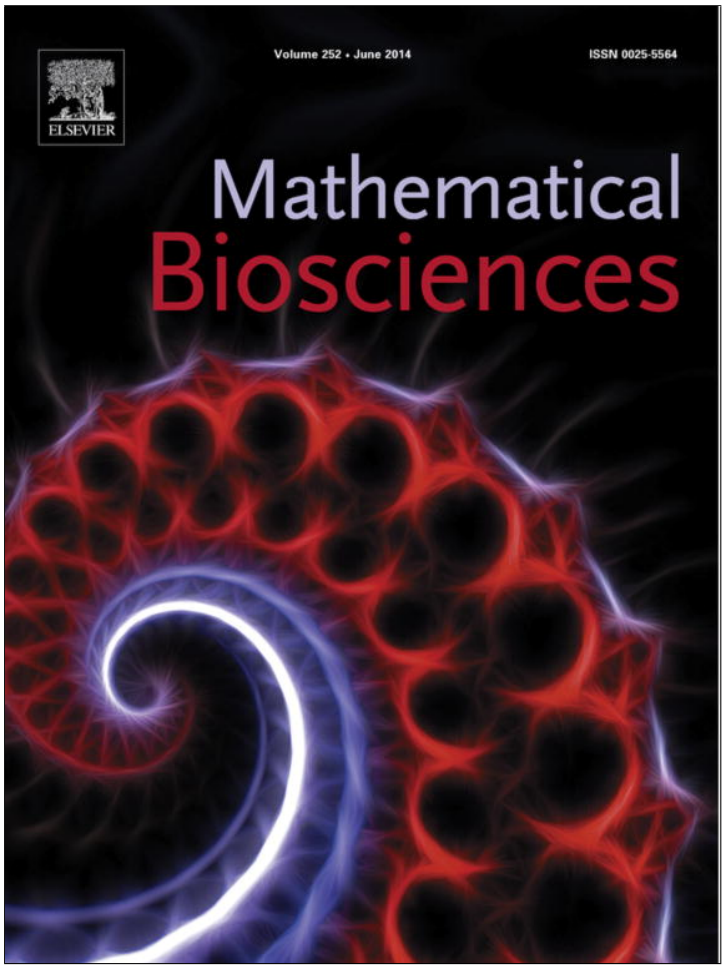

Mathematical Biosciences 252 (2014) 27–35

Contents lists available at ScienceDirect

Mathematical Biosciences

journal homepage: www.elsevier.com/locate/mbs

The lifetimes of small arterial gas emboli, and their possible connection to Inner Ear Decompression Sickness

J.M. Solano-Altamirano *, Saul Goldman

Dept. of Chemistry, The Guelph-Waterloo Centre for Graduate Work in Chemistry and The Guelph-Waterloo Physics Institute, University of Guelph, Guelph, Ontario N1G 2W1, Canada

ARTICLE INFO

Article history:
Received 17 September 2013
Received in revised form 21 January 2014
Accepted 7 March 2014
Available online 21 March 2014

Keywords:
Right/left shunting
Diffusion and Laplace equations
Inner Ear Decompression Sickness
Arterial gas embolus lifetime
Neumann and Dirichlet boundary conditions
Moving gas/liquid boundary

ABSTRACT

We solved both the Diffusion and Laplace equations which predicted very similar results for the problem of a dissolving small gas bubble suspended in a liquid medium. These bubbles dissolved both because of surface tension and solute concentration effects. We focused on predicting bubble lifetimes ("t_d"), and dissolution dynamics — radius *vs* time (R *vs* t) for these contracting bubbles. We also presented a direct comparison of the predicted results, obtained by applying either Dirichlet or Neumann boundary conditions, to the bubble/medium interface. To the best of our knowledge, this is the first direct comparison that has ever been published on the application of these different boundary conditions to a moving gas/liquid boundary. We found that the results obtained by applying either Dirichlet or Neumann boundary conditions were very similar for small, short-lived bubbles ($R_0 < 25$ μ, $t_d < 40$ s), but diverged considerably for larger, longer-lived bubbles. We applied our expressions to the timely problem of Inner Ear Decompression Sickness, where we found that our predictions were consistent with much of what is known about this condition.

1. Introduction

1.1. Decompression Sickness, arterial gas emboli, and the Diffusion equation

Decompression Sickness (DCS) is a medical problem that can range in severity from very mild to fatal. It can affect a variety of organs and tissues, including the skin, joints, the spinal cord, the brain, the eyes, and the inner ear. When it occurs, it is a consequence of an overly rapid drop in the ambient pressure. Depending on whether the initial ambient pressure is equal to or greater than ~1 atm, it is called hypobaric DCS and hyperbaric DCS, respectively. Hyperbaric DCS arises from overly rapid decompression in scuba diving, while hypobaric DCS arises from overly rapid decompression in aviation and space exploration. While the detailed pathophysiology of DCS is still largely unknown, it is very widely accepted as being due to the formation and/or growth of gas bubbles in the blood and tissues of the body, as a consequence of an overly rapid decompression. There is also a growing consensus that in many forms of DCS, the gaseous bubbles that cause the problem are vascular, as opposed to extravascular.

In this work we mathematically characterize the rates of growth/dissolution, and the dissolution times of small arterial gas emboli (AGEs) by solving the Diffusion equation:

$$\frac{\partial}{\partial t}c(r,\theta,\phi;t) = D\nabla^2 c(r,\theta,\phi;t). \tag{1}$$

In Eq. (1) c is the dissolved solute concentration in the medium, t is time, D is the diffusion constant, (r,θ,ϕ) are the spherical coordinates of an infinitesimal volume element in the medium, and ∇^2 is the Laplacian operator.

1.2. Arterial gas emboli (AGE)

Most AGEs *per se*, in the absence of decompression, are small, dissolve rapidly, and do not cause DCS. It is currently believed that many (if not most or all) people have small AGEs present in their arterial circulation. Because of the effects of both dissolved gas under-saturation of arterial blood (below), and surface tension (Eq. (2)), AGEs are thermodynamically unstable, and will dissolve:

$$P_b = P_e + \frac{2\gamma}{R}. \tag{2}$$

Eq. (2) is the well-known Young–Laplace equation, wherein P_b is the gas pressure inside the bubble, P_e, the external pressure, is the pressure in the medium that surrounds the bubble, γ is the surface tension of the bubble/medium interface, and R is the radius of the

* Corresponding author. Tel.: +1 5192653017.
E-mail addresses: jmsolanoalt@gmail.com (J.M. Solano-Altamirano), sgoldman@uoguelph.ca (S. Goldman).

http://dx.doi.org/10.1016/j.mbs.2014.03.008
0025-5564/

bubble. As will be shown (Fig. 5), small gas bubbles ($R \leq 5$ μ) at low-to-moderate pressures ($P_e \leq 5$ atm), suspended in arterial blood, will dissolve within a few seconds due to these combined effects.

A significant source of these small naturally occurring AGEs is "right-to-left shunting" (r/l shunting). This is the phenomenon whereby small gas bubbles are transferred from venous to arterial circulation. They arise in venous circulation due to the release of excess dissolved inert gas (*e.g.* N_2) from tissues during decompression. If sufficiently small, AGEs remain harmless provided the ambient pressure is fixed, but become potentially problematic if the ambient pressure drops rapidly. R/l shunting occurs because of specific types of abnormalities in the body, which are not rare. These abnormalities include: a *Patent Foramen Ovale* ("PFO"), incomplete bubble elimination by the alveoli, and Arterio-Venous Anastomoses (AVAs). A PFO is a defect in the atrial septum of the heart which allows venous blood, together with suspended venous gas bubbles, to enter the arterial circulation [1]. Incomplete bubble elimination by the alveoli may occur because of inefficient gas exchange by damaged or compromised alveoli [2]. AVAs are blood-passing ducts that act as pulmonary shunts, by allowing venous blood and any bubbles it contains, to bypass the lungs (which normally act as effective filters for venous gas bubbles), and enter the arterial circulation [3]. AVAs are believed to be remnants of fetal pulmonary shunts which (normally) close after birth [3].

As indicated above, small AGEs dissolve rapidly because of both surface tension, and dissolved solute under-saturation, and normally cause no harm. During rapid decompression however, tissues become temporarily supersaturated with respect to the circulating dissolved inert gas. Any AGEs entering the arterial capillaries of these tissues will (because they are under-saturated in inert gas relative to these tissues) become nucleation seeds, which will grow due to the transfer of dissolved inert gas from the contiguous tissue to themselves. If they grow sufficiently, they may cause DCS. They may block arterial circulation to the surrounding tissue (ischemia), thereby depriving them of necessary Oxygen. Also, they may damage delicate tissues by tearing or disrupting them. As discussed below in Section 3, tissue damage of this kind has been suggested as an explanation for the poor treatment outcomes found for Inner Ear Decompression Sickness ("IEDCS") [4].

In this work, we will focus on developing tractable approximate models for predicting the dynamics of AGE contraction, and their dissolution time. These AGEs will be modeled as spherical gas bubbles containing air, embedded in a liquid, for which Eq. (2) of applies. Because of the timeliness and importance of IEDCS, we will focus on the possible connection of AGE lifetimes to this condition.

1.3. Solute transport via diffusion and mixing

A significant uncertainty in this work stems from the fact that circulating arterial blood is not static, but is a flowing medium. Dissolved gas transport in the vicinity of a growing/contracting bubble embedded in such a medium will involve convection (*aka* "mixing") and diffusion, as opposed to diffusion alone. This difficulty, which is ubiquitous in applications of the Diffusion equation to physically realistic problems, was first pointed out by Epstein and Plesset in their seminal paper on the application of the Diffusion equation to an air bubble in water [5]. Their particular resolution was to simply state that their result for the dissolving time (in which the unknown effect of mixing was omitted) represented an upper bound on its correct value [5].

While the problem of quantitatively working out the relative contributions of diffusion and mixing in physically realistic problems remains largely unsolved, some progress has been made over the last few decades. Specifically, the so-called "two-region model" used by Epstein and Plesset, is now often replaced by a three-region model, of the kind illustrated in Fig. 1 [6]. The idea is to simplify the solute transfer problem by physically separating the regions wherein diffusion and mixing occur. As shown in the three-region model in Fig. 1, diffusion alone is assumed to occur in the spherical shell of thickness $(H - R)$ that surrounds the bubble. Mixing alone is assumed to occur in the outer so-called "well-stirred region" (WSR), which is an outer spherical shell that surrounds and encloses the diffusive region. In the WSR there are no solute concentration gradients, by definition. Thus, by increasing or decreasing the thickness $(H - R)$ of the inner shell, one respectively increases or decreases the relative contribution to solute transport made by pure diffusion.

2. Theory

Our main objective in this section is to derive explicit expressions for the time-evolution of the radius of an AGE, and its dissolution time, given a prescribed initial state, external pressure $P_e(t)$, and concentration $c_m(t)$ in the WSR (or, equivalently, at $r = H$ in the Diffusive region — see Fig. 1).

While the Diffusion equation *per se* can be viewed as exact in the linear response regime, particular solutions of it can be obtained only after specifying the relevant boundary conditions, which are physically-based, and are often approximations of reality. While $c_m(H, t)$ can be specified from the basis of the arterial gas equation (Eqs. (23) and (24), below), $c_b(R, t)$ cannot. The latter requires the further assumption that Henry's law [7]:

$$c_b(R,t) = \frac{P_b(t)}{K_H} = \frac{1}{K_H}\left(P_e(t) + \frac{2\gamma}{R}\right) \tag{3}$$

applies to the gaseous solute (which here will be approximated by air) at the bubble interface.

The Henry's law constant "K_H" provides the ratio of a solute's partial pressure in a gas to its concentration in solution, *when the solute is in thermodynamic equilibrium with respect to the two phases* [7]. Since the dissolution of an AGE is a non-equilibrium process, there is no basis for assuming that Henry's law applies at the surface of the shrinking bubble. Nevertheless, with the exception of one important recent article [8], in all previous work done on this

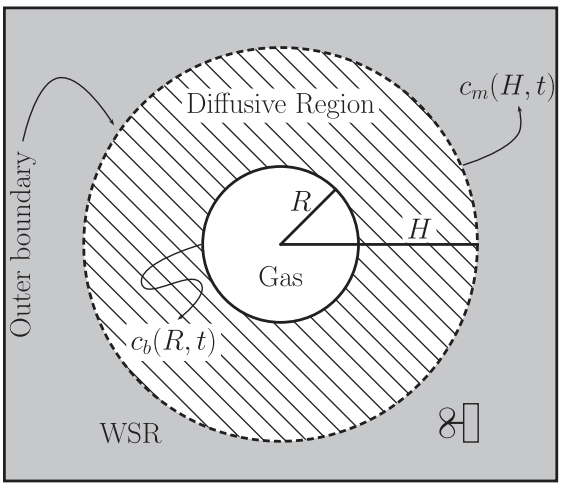

Fig. 1. Physical model of a bubble surrounded by a diffusive medium, which is surrounded by a well-stirred region ("WSR") shown in grey. For two-region models, $H \to \infty$, and for three-region models H is finite. c_b is time-dependent, because (in this work) the bubble continuously contracts with time. c_m is a constant when the ambient pressure is constant, but is time-dependent, when the ambient pressure is time-dependent (such as during an ascent).

problem, Henry's law was invariably assumed to apply at the bubble interface (see Ref. [6], and references therein).

The article referred to above describes the novel approach to the problem taken by Mohammedein and Mohamed [8]. These authors applied Neumann boundary conditions — as opposed to Dirichlet boundary conditions — at the bubble's surface, thereby avoiding the need to assume that Henry's law applies at this surface. The difference between the two is that while Dirichlet boundary conditions require that the value of a quantity (here $c(R,t)$) be specified at all times at the boundary, Neumann boundary conditions require that the values of a normal gradient (here $(\partial c/\partial r)_R$) be specified at all times at the boundary [9, (a)].

While the work in [8] provides a novel solution to the gas bubble problem, it too is not expected to be generally exact. This is because the method in [8] requires the use of a combined variable (or "similarity variable"), in order to separate the Diffusion equation — a partial differential equation — into two ordinary differential equations, which are subsequently solved separately. The exact functional form selected for the combined variable will dictate the form of the bubble growth law (see Eqs. (16)–(19), below). However, the fact that a particular choice for the mathematical form of the combined variable successfully separates the Diffusion equation into two ordinary differential equations does not necessarily mean that the growth law implied by this choice is exact. The growth law arises from "the physics" of the problem.

Since neither the Dirichlet nor the Neumann-based solutions are expected to be generally exact, we will apply them both in this work. It will be shown below, that there exist significant regions of agreement between the predictions of the two methods. The expectation is, that for the problem of interest here, where these fundamentally different methods of solution agree, their predictions are probably correct.

2.1. Derivations based on a Dirichlet boundary condition and Henry's law at the bubble surface

Here we provide derivations for the bubble contraction rate "dR/dt" (which is a time-dependent function), and the dissolution time "t_d" for an AGE, given an initial state, and Dirichlet boundary conditions at the two boundaries of the diffusion region (*i.e.* at $r = R$ and H). The initial state includes the initial bubble radius (R_0), the initial number of moles of solute in the bubble, and the initial solute concentration distribution throughout the diffusion region ($R_0 \leqslant r \leqslant H_0$). Dirichlet boundary conditions apply at all times ($t \geqslant 0$) at both boundaries. Also, Henry's law is assumed to apply at all times, both at the bubble's surface, and in the well-stirred region. Thus, $c(R,t) = c_b(R,t)$, and $c(H,t) = c_m(H,t)$, where $c_b(R,t)$ and $c_m(H,t)$ are obtained, respectively, from Henry's law for air, applied at the bubble surface ($r = R$, and Eq. (3)), and in the well-stirred region ($r = H$, and Eqs. (23) and (24)).

We will provide solutions both of the full Diffusion equation ((1) or (6), below), and of the simpler Laplace equation (Eq. (9), below). The latter is obtained from the former by making the further assumption that a steady-state exists within the diffusion region at all times (Eq. (8), below). As further discussed below, this is equivalent to assuming that a separation of time scales exists, such that the dissolved solute concentration in the diffusion region re-adjusts instantly to any changes in both the bubble radius and the external pressure.

The general strategy is to first derive the connection between dR/dt and $(\partial c/\partial r)_R$. Subsequently, expressions for $(\partial c/\partial r)_R$ are developed which satisfy either the Diffusion or the Laplace equation. For the latter, we will derive expressions for $(\partial c/\partial r)_R$ appropriate to several physical models wherein different diffusion/mixing schemes are assumed.

The connection between dR/dt and $(\partial c/\partial r)_R$ is obtained from Fick's law [10]:

$$\frac{dn}{dt} = \frac{1}{\Re T}\frac{d}{dt}(P_b V_b) = 4\pi R^2 D\left(\frac{\partial c}{\partial r}\right)_R. \tag{4}$$

Here, n is the total number of moles of air in the bubble, D is the diffusion constant of air in the medium, $(\partial c/\partial r)_R$ is the concentration gradient of dissolved air in the medium at R, T is the absolute temperature, and we have used the Ideal Gas law in the middle expression in Eq. (4), with "$\Re$" used to represent the Gas Constant.

Combining Eqs. (2)–(4) gives the desired result:

$$\frac{dR}{dt} = \frac{1}{3P_eR + 4\gamma}\left\{3\Re TDR\left(\frac{\partial c}{\partial r}\right)_R - R^2\frac{dP_e}{dt}\right\}. \tag{5}$$

Different bubble growth/contraction rate laws, and different dissolution time expressions, will arise from using different expressions for $(\partial c/\partial r)_R$ in Eq. (5). The expressions that arise for the latter are a result both of the diffusion model used, and whether the solution is for the Diffusion or the Laplace equation.

We next provide four expressions for $(\partial c/\partial r)_R$, corresponding to each of four different models.

(I) The Diffusion equation under conditions of spherical symmetry is:

$$\frac{\partial c}{\partial t} = D\left(\frac{\partial^2 c}{\partial r^2} + \frac{2}{r}\frac{\partial c}{\partial r}\right). \tag{6}$$

For a Step function initial solute concentration (*i.e.*, $c(R,0) = c_b,\ c(r,0) = c_m,\ H > r > R$), and for $H \to \infty$ and fixed, Epstein and Plesset [5] showed that Eq. (5)

$$\left(\frac{\partial c}{\partial r}\right)_R = (c_m - c_b)\left(\frac{1}{R} + \frac{1}{\sqrt{\pi Dt}}\right) \tag{7}$$

satisfies Eq. (6). We will refer to the model resulting from using Eq. (7) in Eq. (5) as the "DiSIC-HF2" model. The abbreviation stands for "the **Di**ffusion equation, using a **S**tep function for the **I**nitial **C**ondition for the concentration, with **H** **F**ixed, and **2** refers to a two-region model, *i.e.*, $H \to \infty$".

(II) On the other hand, under the steady-state approximation:

$$\frac{\partial c}{\partial t} \equiv \left(\frac{\partial c(r,t)}{\partial t}\right)_r = 0, \tag{8}$$

the Diffusion equation reduces to the Laplace equation:

$$\nabla^2 c(r,t) = \left(\frac{\partial^2 c(r,t)}{\partial r^2}\right)_t + \left(\frac{2}{r}\frac{\partial c(r,t)}{\partial r}\right)_t = 0. \tag{9}$$

The general solution of Eq. (9) for the two-region model (*i.e.* $H \to \infty$) is:

$$c(r,t) = A(t) + \frac{B(t)}{r}, \quad t \geqslant 0,\ r \geqslant R. \tag{10}$$

Here $A(t)$ and $B(t)$ are determined from the values of the dissolved air concentration at the inner and outer boundaries of the diffusion region, *i.e.* from $c_b(R,t)$ and $c_m(H,t)$, respectively.

The physical basis of the steady-state approximation can be appreciated by substituting Eq. (10) into (8). It then becomes clear that this approximation is equivalent to assuming that the rates of bubble growth and external pressure changes are negligible, relative to the rate of solute redistribution in the diffusion region. Also, a key mathematical distinction is that $c(R,t)$ has either explicit or implicit time-dependencies, depending on whether it results from solving the Diffusion or the Laplace equations, respectively.

From Eq. (10), and these boundary conditions, the following expression for the solute concentration gradient normal to the bubble surface at time "t" is obtained:

$$\left(\frac{\partial c}{\partial r}\right)_{r=R,t} = \frac{c_m(t) - c_b(t)}{R(t)}. \tag{11}$$

We will refer to this as the "LHF2" model (**L**aplace equation, (**H**) **F**ixed, **2**-region). By comparing Eqs. (7) and (11) it is evident that neglecting the explicit time-dependent term on the right-hand side of Eq. (7), as Epstein and Plesset did in order to derive their approximate working expressions, is exactly equivalent to solving the Laplace equation for this model. This physical basis for Epstein and Plesset's mathematical approximation has gone unnoticed in previous work.

(III) A plausible alternative is to allow the thickness of the diffusion layer to be related to the bubble radius, as opposed to being independent of it. Therefore, we next introduce a three-region model in which "$H(t)$", the inner radius of the WSR, is made proportional to the radius of the bubble, and thereby time-dependent. We define:

$$H(t) \equiv \lambda R(t), \tag{12}$$

where λ is a constant (> 1). The thickness of the diffusion layer would now not be fixed, but be given by $H(t) - R(t)$, or $R(t)[\lambda - 1]$. It is straightforward to show that for this model,

$$\left(\frac{\partial c}{\partial r}\right)_{r=R,t} = \left(\frac{\lambda}{\lambda - 1}\right)\frac{c_m(t) - c_b(t)}{R(t)}. \tag{13}$$

We will refer to this as the "LHV3" model (**L**aplace equation, (**H**) **V**ariable, **3**-region).

(IV) Another version of a three-region model, which was used by Mohammedein and Mohamed [8], and others (Ref. [6], and references therein), can be constructed by choosing a fixed finite value of H, with $H > R$. For purposes of comparison with the results obtained from using Neumann boundary conditions at the bubble surface, we also solved the Laplace equation for this model, by applying Dirichlet boundary conditions and Henry's law at the bubble surface. This gives:

$$\left(\frac{\partial c}{\partial r}\right)_{r=R,t} = \frac{H}{R(t)}\left(\frac{c_m(t) - c_b(t)}{H - R(t)}\right). \tag{14}$$

We will use the abbreviation "LHF3" for this model, where the meaning of the acronym should now be obvious.

In Table 1 below, we summarize the four models we used that are based on Dirichlet boundary conditions and Henry's law at the bubble/diffusive medium interface.

2.2. Derivations based on Neumann boundary conditions at the bubble surface

This work was described in Ref. [8], to which the reader is referred for details. Here, for purposes of completeness and continuity, we mention a few of the main elements of the method. We also point out two significant differences between our application of this method, and its application in Ref. [8].

One difference is that the work in Ref. [8] was based on the expansion of an AGE, once it is present in an arteriole surrounded by supersaturated tissue. On the other hand, our application is focused on determining the lifetimes of small AGEs as they dissolve and contract in arterial blood, but prior to getting to the supersaturated tissue that ultimately may cause them to inflate.

Another difference is that, unlike in Ref. [8], we will not apply this method to conditions where the ambient pressure "$P_e(t)$", varies with time, such as in an ascent at the end of a scuba dive. This is because if $P_e(t)$ is not constant with time, then neither is the solute concentration in the WSR. This can be seen from Eq. (15) which explicitly shows the time-dependence of $c_m(H,t)$ during an ascent from a scuba dive:

$$c_m(H,t) \equiv c_{art}(t) = \frac{P_{art}(t)}{K_H} \cong \frac{fP_e(t)}{K_H} = f\left(\frac{P_0 - \alpha(t - t_0)}{K_H}\right). \tag{15}$$

As described more fully below K_H, f, $c_{art}(t)$, and $P_{art}(t)$ are respectively, the Henry's law constant for air in arterial blood, the ratio of the dissolved air concentration in arterial blood to its saturation value in arterial blood at pressure P_e, the concentration of dissolved air in arterial blood, and the partial pressure of dissolved air in arterial blood. The problem is that the method of combined variables (or the "similarity method") does not have an analytic solution (of which we are aware), for "$c_m(H,t)$" time-dependent. In Ref. [8] $c_m(H,t)$ was taken as constant both at fixed depths, and during an ascent. Thus, while the solution given for an ascent in Ref. [8] was *mathematically* correct, taking $c_m(H,t)$ to be constant during an ascent is *physiologically* inconsistent with what actually happens during an ascent from a scuba dive. In fact, it is precisely because the demand valve (or regulator) used in scuba diving provides the breathing gas to the diver at ambient pressures at all depths, that scuba diving is possible. Without the demand valve it would be impossible to breath underwater.

2.2.1. Derivation for $R(t)$ and $c(R,t)$ using the similarity method at fixed ambient pressure

Construct a combined variable (or "similarity variable") "s", of the form:

$$s = \frac{\beta r}{R(t)}. \tag{16}$$

Here, r and $R(t)$ have their previous meaning, and β is a constant. When recast in terms of this combined variable, the Diffusion equation under spherical symmetry (Eq. (6)) can be written as:

$$R\frac{dR}{dt} = -\frac{D\beta^2}{s}\left\{\left(\frac{1}{\left(\frac{\partial c}{\partial s}\right)}\right)\frac{\partial^2 c}{\partial s^2} + \frac{2}{s}\right\} = \frac{A}{2}. \tag{17}$$

Integration of this equation over R and t is trivial, giving

$$R^2 = At + B. \tag{18}$$

Using $R(0) = R_0$ and $R(t_d) = 0$, where t_d denotes the dissolution time, one finds:

Table 1
Abbreviations used for four models, and the corresponding expressions for $(\partial c/\partial r)_R$.

Model abbreviation	Description	Equation for $(\partial c/\partial r)_R$
DiSIC-HF2	Uses solution of Diffusion equation with a Step IC, two regions (fixed $H = \infty$).	(7)
LHF2	Uses solution of Laplace equation, two regions (fixed $H = \infty$).	(11)
LHV3	Uses solution of Laplace equation, three regions (variable $H, H(t) = \lambda R(t)$).	(13)
LHF3	Uses solution of Laplace equation, three regions (fixed finite H).	(14)

$$R(t) = R_0\sqrt{1-\frac{t}{t_d}} \tag{19}$$

for the time-dependence of the radius of a dissolving bubble.

Using Eqs. (16) and (17), and following a similar procedure as was used in Ref. [8], it can be shown that the solution of the Diffusion equation for the dissolved solute concentration in the medium at the bubble surface is given by:

$$c(R(t),t) = c_m + \exp\left(\frac{A}{4D}\right)\left\{\frac{A}{4D}(3P_eR+4\gamma)\right\} \times\left\{\frac{R}{H}\exp\left(-\frac{AH^2}{4DR^2}\right)-\exp\left(-\frac{A}{4D}\right)+\sqrt{\frac{\pi A}{4D}}\left[\operatorname{erf}\left(\frac{H}{R}\sqrt{\frac{A}{4D}}\right)-\operatorname{erf}\left(\sqrt{\frac{A}{4D}}\right)\right]\right\}. \tag{20}$$

Here A is a constant that is determined numerically (*e.g.* by the Newton–Raphson method) after setting $t = t_0$. In arriving at Eq. (20), we used a finite constant value of H and took the ambient pressure to be fixed. Eq. (20) was used to determine $c(R,t)$, the behavior of which is illustrated in Fig. 3.

3. System

3.1. Approximations for arterial blood, it's dissolved gases, and the contents of the bubble

Arterial blood in humans is a highly complex fluid which, at a total alveolar (or external) pressure of 760 mm Hg (1 atm), consists of 570 mm N_2 (~76%), 95 mm O_2 (~13%), 46 mm H_2O (~6%), and 40 mm CO_2 (~5%), in addition to its non-volatile constituents [2]. The these partial pressures sum to 751 mm Hg, which indicates that arterial blood is slightly under-saturated *i.e.* $(751/760 = 0.988) < 1$, with respect to its gaseous constituents. This slight (over-all) under-saturation is due to a ventilation-perfusion ratio that is less than one. This causes a reduced oxygen partial pressure in arterial blood, relative to its alveolar value (95 mm Hg in arterial blood *vs* 104 mm Hg the alveoli [2]). The complexity of the problem is further exacerbated by the fact that the arterial partial pressures of N_2 and O_2 increase with their increasing alveolar pressures, while the partial pressures of CO_2 and H_2O are almost constant, and constant, respectively [2,12].

It would be extremely difficult (if not impossible) to solve the Diffusion equation for a bubble containing a multicomponent gaseous mixture manifesting this level of complexity. However, it is not necessary to do this for our purpose, which is to estimate the temporal dissolution pattern of the bubble (R *vs* t), and its dissolution time. For given initial conditions, these functions are largely determined by the *overall* degree of under-saturation, the average values of the underlying physical constants, and by the surface tension of the bubble.

Consequently, we will approximate the gas mixture dissolved in arterial blood, and which fills the AGE, by air (taken to be a 1-component gas). Also, the physical constants for air in water at 37 °C (the Henry's law constant and the Diffusion constant), will be used in place of the values for the actual constituent gases in arterial blood (some of which are unknown). Thus, arterial blood will be assumed, at all external pressures, to contain a partial pressure of dissolved air that is 0.988 of its saturation value, and the bubble will be assumed to consist of pure air, whose total pressure is given by Eq. (2). The working expressions resulting from this model are given below around Eqs. (23) and (24).

3.2. The application

We focus on small, short-lived AGEs arising from r/l shunting, and their possible relation to IEDCS. We chose to focus on small, short-lived AGEs for physical reasons that are described below. This particular medical condition was selected both because its importance and timeliness in diving medicine.

Recently, Klingmann [4] reported the results of a clinical study wherein almost 75% of recreational scuba divers breathing air, and diving conservatively, who were diagnosed with IEDCS, also had an r/l shunt. This followed an earlier study in which 82% of the IEDCS patients were reported to have had an r/l shunt [11]. Klingmann suggested that the pathophysiology of IEDCS very likely involved AGEs getting to the arterioles of the inner ear, and that during decompression, the transfer of excess N_2 from contiguous super-saturated tissue to the AGE(s) causes the AGE(s) to inflate.

Unfortunately, IEDCS very often has a poor treatment outcome when treated by standard recompression therapy, *i.e.*, it usually results in some degree of permanent hearing loss. Klingmann suggested that this may be a consequence of irreversible tissue damage to the very thin membranous structures of the vestibular region in the inner ear, which may be intolerant to local bubble growth.

The physical reason for choosing to work with small AGEs was that our boundary conditions — both Dirichlet and Neumann — are likely to be correct for small short-lived AGEs, but incorrect for larger, longer-lived AGEs. As will be shown in Section 5, both Dirichlet and Neumann boundary conditions, each applied with their respective approximations at the bubble/medium interface, predicted very similar contraction rates and dissolution times for small (< 25 μ) short-lived (< 40 s) AGEs. But their predictions diverged as the initial size and lifetimes of the AGEs increased significantly beyond these values. Therefore, in order to be reasonably confident in the validity of our predictions, we chose to focus on these small short-lived AGEs for which both methods agreed.

4. Calculations

4.1. Analytic working equations for the LHF2, LHF3 and LHV3 models

These are based on solving the Laplace equation using Dirichlet boundary conditions, Henry's law at the bubble surface, and a fixed ambient pressure.

4.1.1. LHF2

Substituting the expression for $(\partial c/\partial r)_R$ given by Eq. (11) into Eq. (5), and considering the ambient pressure to be constant, we find

$$3Dd\cdot dt = \frac{3P_eR^2+4R\gamma}{RP_e(f-1)-2\gamma}dR, \tag{21}$$

where

$$d \equiv \Re T/K_H. \tag{22}$$

In arriving at Eq. (21), we used the fact that arterial blood is slightly under-saturated with respect to its dissolved gaseous solutes. Therefore $c_m(H,t)$ will be given by "c_{art}", the dissolved concentration of air in arterial blood which, in turn, is obtained from Henry's law:

$$c_m(H,t) = c_{art} = \frac{P_{art}(t)}{K_H}. \tag{23}$$

In Eq. (23), K_H is the Henry's law constant for air in arterial blood, and $P_{art}(t)$ is the total pressure of the dissolved arterial gases. It is related to the ambient pressure P_e by

$$P_{art}(t) = fP_e(t) \cong (751/760)P_e = 0.98816P_e \tag{24}$$

from which it is obtained. Here "f" stands for the factor by which the medium is under-saturated with respect to its dissolved volatile solute.

After integrating Eq. (21), we find

$$t = -\frac{R^2 - R_0^2}{2Dd(1-f)} + \frac{2(2f+1)\gamma(R-R_0)}{3Dd(1-f)^2 P_e} - \left\{ \frac{4(2f+1)\gamma^2}{3Dd(1-f)^3 P_e^2} \times \ln\left(\frac{(1-f)P_e R + 2\gamma}{(1-f)P_e R_0 + 2\gamma} \right) \right\}. \quad (25)$$

Eq. (25) cannot be inverted analytically, because it is transcendental. But since the right-hand side of Eq. (25) is a monotonically smooth decreasing function of R, a simple Newton–Rhapson method [9, (b)] can be used to invert the equation, in order to get $R(t)$ *vs* t, to any desired level of precision. Alternately, one can determine t as a function of R ($0 \leqslant R \leqslant R_0$) by using Eq. (25), and switching the axes $t \leftrightarrow R$. The second method which is faster, and free of numerical error, was used to produce the insets shown in the figures.

By setting $R = 0$ in Eq. (25), one obtains the dissolving time "t_d" explicitly as a function of the initial bubble radius "R_0", and other known constants.

4.1.2. LHF3

To get the corresponding expressions for the LHF3 model, one substitutes Eq. (14) into Eq. (5) which gives:

$$3DdH \cdot dt = \frac{\left(3P_e R^2 + 4\gamma R\right)(H-R)}{P_e R(f-1) - 2\gamma} dR. \quad (26)$$

Integrating Eq. (26), and using Eqs. (23) and (24) as above, gives:

$$t = \frac{R^3 - R_0^3}{3DdH(1-f)} - \left[\frac{1}{2Dd(1-f)} + \frac{(2f+1)\gamma}{3DdH(1-f)^2 P_e} \right]\left(R^2 - R_0^2\right) + \left[\frac{2(2f+1)\gamma}{3Dd(1-f)^2 P_e} + \frac{4(2f+1)\gamma^2}{3DdH(1-f)^3 P_e^2} \right](R - R_0) - \left\{ \left[\frac{4(2f+1)\gamma^2}{3Dd(1-f)^3 P_e^2} + \frac{8(2f+1)\gamma^3}{3DdH(1-f)^4 P_e^3} \right] \times \ln\left(\frac{(1-f)P_e R + 2\gamma}{(1-f)P_e R_0 + 2\gamma} \right) \right\}. \quad (27)$$

Again, setting $R = 0$ in Eq. (27), gives the working expression for t_d explicitly as a function of R_0, and other known constants.

4.1.3. LHV3

By substituting

$$D \to D' = \frac{\lambda}{\lambda - 1} D, \quad (28)$$

into Eq. (25), one obtains its analogue for the LHV3 model, and on setting $R = 0$, we again get an explicit expression for t_d as a function of R_0 (and other known constants), for the LHV3 model.

As expected, the above solutions obtained for the three-region models, LHV3 and LHF3, correctly reduce to the corresponding two-region LHF2 model solutions, on taking the limits $\lambda \to \infty$, and $H \to \infty$, respectively.

4.1.4. Varying ambient pressure

When the ambient pressure is time-dependent, as it is during an ascent from a dive, it is not possible to analytically integrate the rate expressions as we did in the previous section. Therefore for the examples involving a variable ambient pressure (Fig. 5, below) the integration of Eq. (5) was done numerically, using 4th-order Runge–Kutta integration, together with Eqs. (29) and (30), below. Further details are outlined in Section 4.2.

For constant rates of ascent, the ambient pressure has the form

$$P_e(t) = P_0 - \alpha(t - t_0), \quad (29)$$

where P_0 is the ambient pressure at the start of the ascent *i.e.* at $t = t_0$, and α is the (constant) rate of decompression. For a fixed depth (or at the surface), $\alpha = 0$, and for finite ascent rates, α (in units atm/s) is given by

$$\alpha = \frac{1 \text{ atm}}{33 \text{ fsw}} \frac{dZ}{dt}, \quad (30)$$

where $dZ/dt \geqslant 0$ is the constant ascent rate (in fsw/s, and fsw stands for "feet sea water"). Eq. (30) is based on the equivalence: 1 atm corresponds to 33 fsw.

For constant descent rates, one would also use Eq. (29), but with a positive sign in front of the 2nd term on the right-hand side.

4.2. Numerical working equations for the four models based on Dirichlet boundary conditions, Henry's law at the bubble surface, and a fixed or variable ambient pressure

We start by first considering the Diffusion equation which requires particular care, and subsequently generalize the result to the three Laplace equation-based models.

Substituting Eq. (7) into Eq. (5) gives:

$$\frac{dR}{dt} = \frac{RP_e(f-1) - 2\gamma}{3P_e R^2 + 4\gamma R}\left[3Dd\left(1 + \frac{R}{\sqrt{\pi D t}} \right) \right]. \quad (31)$$

Eq. (31), as written, cannot be integrated either analytically or numerically. Numerical integration is unstable due to two singularities which occur at the extremities of the integration range, *i.e.* at $(R = R_0;\ t = 0)$, and at $(R = 0;\ t = t_d)$.

The singularity at $(R = R_0;\ t = 0)$ is removed by transforming $t \to s^2$, and the singularity at $(R = 0;\ t = t_d)$ is removed by changing the function that is integrated from the bubble radius R, to the number of moles of air in the bubble "n".

On transforming $t \to s^2$, Eq. (4) becomes:

$$\frac{dn}{ds} = 8\pi R^2 D\left\{ s\left(\frac{\partial c}{\partial r} \right)_R \right\}. \quad (32)$$

Eq. (32) is applicable to all four models using Dirichlet boundary conditions at the bubble surface, and is valid both for fixed and variable ambient pressures.

Combining Eq. (2) with the Ideal Gas law gives:

$$R^3 + \frac{2\gamma R^2}{P_e} - \frac{3n\Re T}{4\pi P_e} = 0, \quad (33)$$

which provides R at all values of n through an exact solution of this cubic equation.

Substituting Eq. (7) into Eq. (32) gives:

$$\frac{dn}{ds} = 8\pi D\left\{ \frac{RP_e(f-1)}{K_H}\left(s + \frac{R}{\sqrt{\pi D}} \right) \right\} \quad (34)$$

for the transformed Diffusion equation. Eq. (34) is everywhere well-behaved, and readily integrated using standard methods, such as a 4th-order Runge–Kutta procedure.

The same approach is used to obtain the working equations for the LHF2, LHV3 and LHF3 models, at variable ambient pressures. Specifically, substituting Eqs. (11), (13) and (14) for $(\partial c/\partial r)_R$ into Eq. (32) gives stable, numerically integrable equations for the LHF2, LHV3 and LHF3 models, respectively. These equations are applicable at both fixed and variable ambient pressures.

4.3. Accuracy of numerical integrations

We checked the accuracy of our numerical integrations at fixed ambient pressures for the Laplace-based equations, by comparing them with the analytic results provided by Eqs. (25) and (27). In this way, we verified that the numerical errors were those expected for the 4th-order Runge–Kutta method. Specifically, the

relative errors obtained oscillated around $10^{-5} - 10^{-4}$, which is very small, in relation to our requirements.

5. Results

Our results are given graphically in Figs. 2–5.

Fig. 2 illustrates the differences found by solving the Laplace equation, as opposed to the full Diffusion equation, for a two-region model (*i.e.* $H \to \infty$). The plots are for the dissolution time *vs* the initial bubble radius (main plot), and radius *vs* time (inset), for a dissolving AGE. It is evident that the discrepancy between the two solutions is quite small for the small AGEs shown here. By comparing Fig. 2 with Fig. 4, it is seen that these differences are generally smaller than those that arise from using Neumann, as opposed to Dirichlet boundary conditions. Also, by comparing Fig. 2 with Fig. 5, it is seen that the choice of a pure diffusion model ($\lambda \to \infty$), as opposed to one involving a mix of diffusion and convection ($\lambda = 2$), also creates a much larger discrepancy between these functions, than those shown in Fig. 2. Consequently, we will use the simpler Laplace equation in all our calculations involving Dirichlet boundary conditions at the bubble surface.

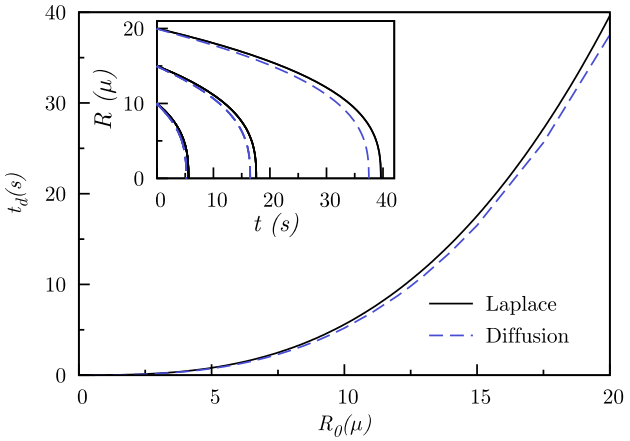

Fig. 2. Comparison of the dissolution time of an AGE, as a function of its initial radius, based on the Diffusion and Laplace equations. The plots were determined using Eq. (25) and ((33), (34)), for the LHF2 and Di-SICHF2 models, respectively (see Table 1 and text for details). Inset: Bubble radius *vs* time for three initial radii. Here $\gamma = 0.7$ μ atm, $f = 0.98816$, $D = 2900\ \mu^2/s$, $d = 0.015768$, $K_H = 1614\ l$ atm/mol, $T = 310.15\ K$, and $P_e = 1$ atm.

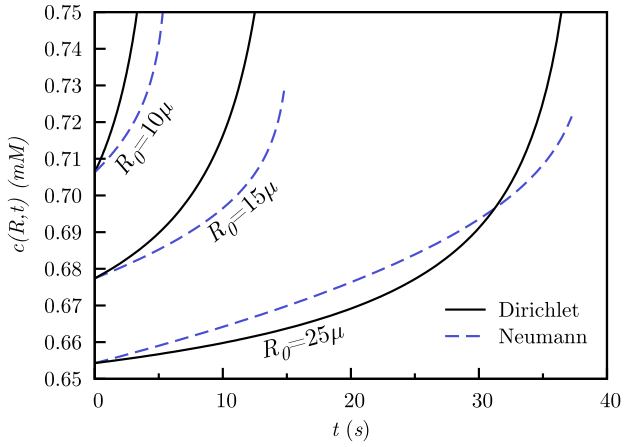

Fig. 3. The effect of applying Neumann *vs* Dirichlet boundary conditions on the calculated dissolved solute concentration at the surface of AGEs of different initial radii. The plots for Neumann and Dirichlet boundary conditions were obtained from Eqs. (19), (20) and Eqs. (3), (27), respectively. The physical constants are the same as for Fig. 2, but the value of H is here finite, and equal to 40 μ. The curves terminate near the dissolution time (t_d) of the AGE.

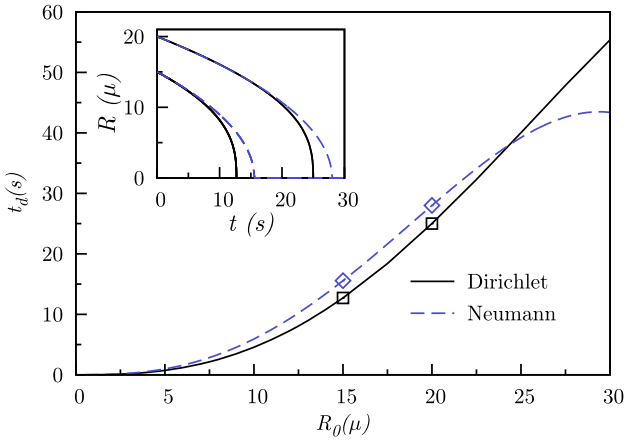

Fig. 4. The predicted dissolution time, and radius *vs* time (inset), for AGEs of different initial radii, using Neumann and Dirichlet Boundary Conditions. The values of R_0 and t_d indicated on the main plots with points correspond to the two time evolution plots shown in the inset. The three-region model with H fixed at 40 μ was used for both boundary conditions (see Table 1 and text for details). Eqs (18), (19), and (27), were used for the Neumann-, and Dirichlet-based plots, respectively, and the constants are those given with Fig. 2.

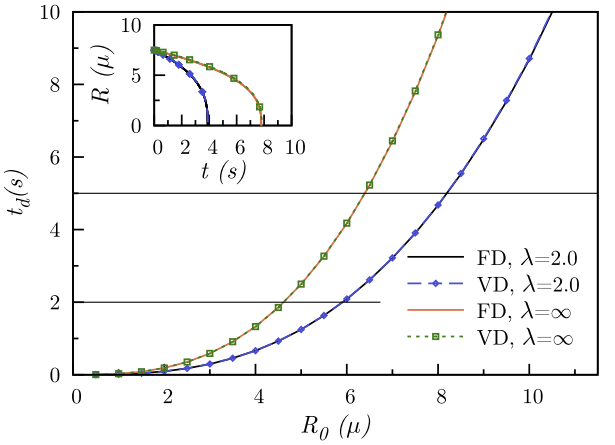

Fig. 5. The dissolution time of an AGE as a function of its initial radius for fixed depths (FD) and variable depths (VD), and for different thicknesses of the diffusion layer. All the plots are based on Dirichlet boundary conditions at the bubble surface, and the plots for variable depths were determined numerically using Eqs. (33), and (34). The plots at fixed depth were determined using Eqs. (25), (28) and Eq. (25), for $\lambda = 2$ and $\lambda = \infty$, respectively.

Fig. 3 shows the deviations from Henry's law obtained by using Neumann boundary conditions. To the best of our knowledge, this is the first time that such a comparison has been published for the problem of a moving gas/liquid boundary. It is seen that the deviations are significant, and can be either positive or negative, depending on the initial radius, and on time. The deviations are here negative for small AGEs ($R_0 \leq 15$ μ), and can be either positive or negative (depending on time) for larger AGEs. Negative and positive deviations mean that the dissolved solute concentration at the bubble surface will be, respectively, smaller and larger than the values based on Henry's law. Smaller and larger solute concentrations at the bubble surface will lead to slower and faster dissolution, respectively (see for example, Eq. (4)). This means that when Henry's law is not imposed at the bubble surface, small AGEs will always be predicted to dissolve more slowly, relative to the corresponding Henry's law-based predictions. Larger AGEs will dissolve

either more slowly, or more rapidly, depending on their size and time.

This is illustrated in Fig. 4 which shows a cross-over in the t_d *vs* R_0 plots. The plots shown were generated by using Neumann (dashed lines) or Dirichlet boundary conditions (solid lines), at the bubble surface. These plots show that for AGEs with $R_0 \leq 25$ μ, both methods predict similar values both for the AGE dissolution dynamics (insets), and for the dissolution times t_d (main graphs). For larger bubbles, however, the predictions stemming from the two boundary conditions deviate significantly.

Fig. 5 shows a result that may help account for the observation that IEDCS frequently occurs unexpectedly, *i.e.* when the dive was within the prescribed time-depth limits, and the diver ascended at an appropriate ascent rate. Colloquially, IEDCS often occurs as an "undeserved hit".

For each value of λ in Fig. 5, we show two plots, one (solid lines, "FD") is for an AGE that evolves at a fixed depth of 100 fsw. The other (dashed lines plus points, "VD") is for an AGE that evolves during an ascent at a (typical) rate of 1 fsw/s, from 100 fsw, with the AGE initially created at 100 fsw. Note that for the initial radii and dissolution times shown here, the bubble dynamics (inset) and dissolution times (main graph) are virtually indistinguishable for fixed depths and ascents. This occurs partly because, for these small bubbles and rapid dissolution times, very little fractional change in the ambient pressure occurs during the bubble's lifetime, and partly because of the opposite effects manifested by R and $(\partial c/\partial r)_R$ on the contraction rate of a bubble (see Eqs. (4), (7), (11), (13) and (14)).

The horizontal lines drawn at 2 and 5 s represent the estimated exposure times of an AGE to arterial blood, for an AGE produced by passage through a PFO, and an AVA, respectively. The exposure time is the total time that the AGE is exposed to arterial blood, from the time it passes the r/l shunt, until the time it reaches the Labyrinthine artery in the head. The details by which these estimates were arrived at are given in Appendix A.

For definiteness, consider first the horizontal at 2 s. This horizontal intersects the $\lambda = 2$ plots at ≈ 6 μ. This means that an AGE originating from a PFO at 100 fsw will survive to reach the inner ear, if it's initial radius is greater than ≈ 6 μ, but it will have fully dissolved prior to reaching the inner ear, if it's initial radius is less than ≈ 6 μ. The $\lambda = \infty$ plots were included in this graph, in order to put a lower bound on this estimate. These plots, because they are for pure diffusion, provide the maximum dissolution time (*i.e.* an upper bound on t_d) for an AGE of a given initial radius, created at a given depth. The 2 s horizontal intersects the $\lambda = \infty$ plots at ≈ 4.5 μ. Taken together, these results indicate that an AGE from a PFO generated at 100 fsw, will survive it's trip to the inner ear if it's initial radius is greater than $\approx (4.5–6)$ μ, but it will have fully dissolved before reaching the inner ear if it's initial radius is less than $\approx (4.5–6)$ μ.

Repeating this exercise for the horizontal at 5 s, we find that an AGE from an AVA generated at 100 fsw, will survive it's trip to the inner ear if its initial radius is greater than $\approx (6–8)$ μ, but it will have fully dissolved before reaching the inner ear if it's initial radius is less than $\approx (6–8)$ μ.

6. Summary

The Diffusion and Laplace equations were solved to determine the dissolution times, and the bubble-radius *vs* time dissolution curves, for small gas bubbles suspended in a liquid medium. These bubbles dissolved due to the effects of surface tension and dissolved solute under-saturation. The differences that resulted from the application of one or the other of these equations were small and totally insignificant for our purposes.

We also carried out the first comparison (of which we are aware), between the results obtained for this problem by separately applying Neumann and Dirichlet boundary conditions at the bubble's surface. We found that these two boundary conditions predicted very similar results, provided the bubbles were small (< 25 μ) and short-lived (<40 s), but diverged significantly for larger longer-lived bubbles.

We applied our rate expressions to the timely (and serious) problem of Inner Ear Decompression Sickness (IEDCS). This is believed to be caused by small arterial gas emboli (AGEs) which get into arterial circulation via a right-left shunt. Subsequently, they are believed to get to the arterioles of the inner ear, where they become inflated with inert gas during decompression. The inert gas comes from the contiguous supersaturated tissues of the inner ear.

A key point in our analysis was to compare AGE exposure times to arterial blood "t_{exp}", with their dissolution times in arterial blood "t_d". The idea is that if an AGE dissolved before reaching the Labyrinthine artery in the head (*i.e.* if $t_d < t_{exp}$), IEDCS would not occur. If however, it survived the trip to this artery (*i.e.* if $t_d > t_{exp}$), IEDCS may occur.

The dissolution time "t_d" is influenced by the depth at which the AGE is created — the greater the depth, the greater the number of moles of gas in the AGE — and by its initial radius "R_0". We found that "t_d" was (for typical diving ascent rates), almost independent of the rate of ascent. Therefore (for typical diving ascent rates), for an AGE created by passage through an r/l shunt at a particular depth, reducing the ascent rate has virtually no effect on "t_d". Consequently, reducing the ascent rate has no bearing on whether or not an AGE gets to the inner ear before it dissolves. For an AGE created at a particular depth, this depends almost entirely on the AGE's initial radius"R_0". This, in turn, will depend on the whether the diver has a medically significant (*i.e.* large) r/l shunt.

Our predictions are consistent with much of what is known about IEDCS. Specifically, it frequently occurs after what was considered a safe dive followed by a safe ascent, and it is much more common in divers with a right-left shunt, than in divers without such a shunt. As indicated in the preceding paragraph, for small short-lived bubbles, and for typical diving ascent rates, the ascent rate has almost no effect on the dissolution time of the AGE, which (for an AGE created at a particular depth), is governed almost entirely by the initial size of the AGE entering arterial circulation. Therefore, divers with a significant right-left shunt (such a *Patent Foramen Ovale*, or an Arterio-Venous Anastomosis), which allows the passage of relatively large AGEs into arterial circulation, would be expected to be relatively susceptible to IEDCS, which is what is observed clinically.

Acknowledgments

We are grateful to the Natural Sciences and Engineering Research Council of Canada (NSERC) for financial support in the form of a Discovery Grant to one of us (SG).

Appendix A. Estimation of the exposure time of an AGE to arterial blood

We need estimates for the total exposure time of an AGE to arterial blood, from the time it is passed through an r/l shunt, until the time it reaches the Labyrinthine artery in the head. To do this, we use a rudimentary model of arterial flow, estimates of mean arterial flow rates, and estimates of the dimensions of the relevant arteries. The specific values used were validated elsewhere [13]. We estimate the total exposure time from the sum of the number of cardiac cycles prior to leaving the left heart, and the transit time while in arterial circulation *en route* to the Labyrinthine artery.

Table A.2
Arterial radii and lengths, and linear speed of blood in selected arteries that connect the heart to the head.

Name	Lbl[a]	r_i (cm)	L_i (cm)	v_i (cm/s)	t_i[b] (s)
Ascending aorta	1	1.47	4	12.28	0.326
Aortic arch I	2	2.24	2	5.287	0.378
Brachiocephalic	3	0.699	3.4	54.29	0.063
R. carotid	5	0.473	17.7	118.6	0.149
R. ext. carotid	13	0.382	17.7	181.8	0.097
L. carotid	15	0.413	20.8	155.5	0.134
L. ext. carotid	17	0.334	17.7	237.9	0.074

[a] The labels are from Ref. [13].
[b] This is the time a differential volume element takes to traverse the artery, as obtained with Eq. (A.2).

Only the main arteries are considered, since flow through arterioles — as measured by the linear velocity — is extremely rapid. Our model of the main arteries consists of joined cylinders of different lengths and diameters. We ignore the true shape of the arteries and of the arterial interconnections, the periodic nature of arterial flow, and assume the constant average volumetric flow rate of arterial blood to be 5 l/min (or 83.3 cm^3/s) [13].

The linear velocity of a fluid "v_i" is related to its flow rate "q" by

$$v_i = \frac{q}{A_i} = \frac{q}{\pi r_i^2}. \tag{A.1}$$

Here, A_i is the cross-sectional area of artery "i" (taken to be a cylinder of radius r_i). The time that it takes an infinitesimally small volume element of blood to traverse an artery of length L_i is obtained from

$$t_i\ (\mathrm{s}) = \frac{L_i \pi r_i^2}{q} = \frac{L_i \pi r_i^2}{83.3\ \mathrm{cm}^3/\mathrm{s}}, \tag{A.2}$$

where the length and radius of the artery are in cm.

The dimensions of the relevant arteries, and the times required to traverse each of them are entered in Table A.2.

(1) Exposure time for an AGE passed through a PFO.
From this table the total transit time is.635 s (using arteries 1, 3, 5, 13) and.912 s (using arteries 1, 2, 15, 17) to the left and right ears, respectively. We average these, and round up the average value to 1 s, as the approximate transit time to either ear from the left heart.
We estimate that an AGE passed through a PFO into the left heart remains there for 1 cardiac cycle, prior to entering the Ascending aorta. Assuming that a cardiac cycle takes 1 s, we obtain an estimate of 2 s for the total exposure time to arterial blood experienced by an AGE from a PFO reaching the Labyrinthine artery in the head.

(2) Exposure time for an AGE created by the passage of a venous bubble through an AVA.
The exposure time to arterial blood will here be somewhat longer than for a PFO-generated AGE, because venous bubbles coming from the right heart and passed through an AVA, require at least 4 cardiac cycles before they appear in the left heart [3]. This is the time required for the venous bubble to go from the right heart, through the AVA, and into the left heart. We assume, on average, 5 cardiac cycles, or 5 s are required for the transit from the right heart through the AVA to the left heart. Assuming half this time was spent in venous, and half in arterial circulation, we find that we should add 2.5 s to the arterial blood exposure time, beyond what it was estimated to be for an AGE passed through a PFO. Consequently, our estimate of the total exposure time of an AGE originating from the passage of a venous bubble through an AVA is 4.5 s, which we round up to 5 s.

References

[1] R.E. Moon, E.M. Camporesi, J.A. Kisslo, Patent foramen ovale and decompression sickness in divers, Lancet 333 (8637) (1989) 513.
[2] R.D. Vann, Inert gas exchange and bubbles (Chapter 4), and mechanism and risks of decompression sickness (Chapter 7), in: A.A. Bove, J.C. Davis (Eds.), Diving Medicine, fourth ed., Saunders, 2004.
[3] M. Ljubkovic, J. Zanchi, T. Breskovic, J. Marinovic, M. Lojpur, Z. Dujic, Determinants of arterial gas embolism after scuba diving, J. Appl. Physiol. 112 (2012) 91.
[4] C. Klingmann, Inner ear decompression sickness in compressed-air diving, Undersea Hyperb. Med. 39 (1) (2012) 589.
[5] P.S. Epstein, M.S. Plesset, On the stability of gas bubbles in gas–liquid solutions, J. Chem. Phys. 18 (1950) 1505.
[6] P. Tikuisis, W.A. Gerth, Decompression theory, in: A.O. Brubakk, T.S. Neuman (Eds.), Bennett and Elliott's Physiology and Medicine of Diving, fifth ed., Saunders, 2003 (Chapter 10.1).
[7] I.M. Klotz, Chemical Thermodynamics, Benjamin, 1964. pp. 336–355.
[8] S.A. Mohammedein, K.G. Mohamed, Concentration distribution around a growing gas bubble in tissue, Math. Biosci. 225 (2010) 11.
[9] W.H. Press, B.P. Flannery, S.A. Teukolski, W. Vetterling, Numerical Recipes, The Art of Scientific Computing (FORTRAN Version), Cambridge University Press, 1989 ((a) 516 (b) 257).
[10] J.A. Jacquez, Compartmental Analysis in Biology and Medicine, second ed., vol. 12, The University of Michigan Press, 1985.
[11] E. Cantais, P. Louge, A. Suppini, P.P. Foster, B. Palmer, Right-to-left shunt and risk of decompression illness with cochleovestibular and cerebral symptoms in divers: case control study of 101 consecutive dive accidents, Crit. Care Med. 31 (2003) 84.
[12] S. Goldman, A new class of biophysical models for predicting the probability of decompression sickness in scuba diving, J. Appl. Physiol. 103 (2007) 484.
[13] P. Wilmhurst, J.J. Wang, K.H. Parker, Wave propagation in a model of the arterial circulation, J. Biomech. 37 (2004) 457 (and references therein).